

Effects of primary aberrations on the fluorescence depletion patterns of STED microscopy

Suhui Deng,^{1,2} Li Liu,^{1*} Ya Cheng,¹ Ruxin Li,¹ and Zhizhan Xu¹

¹State Key Laboratory of High Field Laser Physics, Shanghai Institute of Optics and Fine Mechanics, Chinese Academy of Sciences, Shanghai 201800, China

²Graduate University of Chinese Academy of Sciences, Beijing 100039, China

* Lily_liu@siom.ac.cn

Abstract: Effects of primary aberrations including spherical aberration, coma and astigmatism on the three fluorescence depletion patterns mainly used in stimulated emission of depletion (STED) microscopy are investigated by using vectorial integral. The three depletion patterns are created by inserting a vortex phase plate, a central half-wavelength plate or a semi-circular half-wavelength mask within Gaussian beam respectively. Attention is given to the modification of the shape, peak intensity, the central intensity of the dark hole and the hole size of these depletion patterns in the presence of primary aberrations.

©2010 Optical Society of America

OCIS codes: (050.1960) Diffraction theory; (180.0180) Microscopy; (350.5730) Resolution.

References and links

1. S. W. Hell, and J. Wichmann, "Breaking the diffraction resolution limit by stimulated emission: stimulated-emission-depletion fluorescence microscopy," *Opt. Lett.* **19**(11), 780–782 (1994).
2. S. W. Hell, "Far-Field Optical Nanoscopy," *Science* **316**(5828), 1153–1158 (2007).
3. S. W. Hell, "Microscopy and its focal switch," *Nat. Methods* **6**(1), 24–32 (2009).
4. T. A. Klar, E. Engel, and S. W. Hell, "Breaking Abbe's diffraction resolution limit in fluorescence microscopy with stimulated emission depletion beams of various shapes," *Phys. Rev. E Stat. Nonlin. Soft Matter Phys.* **64**(6), 066613 (2001).
5. T. Watanabe, M. Fujii, Y. Watanabe, N. Toyama, and Y. Iketaki, "Generation of a doughnut-shaped beam using a spiral phase plate," *Rev. Sci. Instrum.* **75**(12), 5131–5135 (2004).
6. J. Keller, A. Schönle, and S. W. Hell, "Efficient fluorescence inhibition patterns for RESOLFT microscopy," *Opt. Express* **15**(6), 3361–3371 (2007).
7. K. I. Willig, J. Keller, M. Bossi, and S. W. Hell, "STED microscopy resolves nanoparticle assemblies," *N. J. Phys.* **8**(6), 106 (2006).
8. P. Török, and P. R. T. Munro, "The use of Gauss-Laguerre vector beams in STED microscopy," *Opt. Express* **12**(15), 3605–3617 (2004).
9. D. P. Biss, and T. G. Brown, "Primary aberrations in focused radially polarized vortex beams," *Opt. Express* **12**(3), 384–393 (2004).
10. B. R. Boruah, and M. A. A. Neil, "Susceptibility to and correction of azimuthal aberrations in singular light beams," *Opt. Express* **14**(22), 10377–10385 (2006).
11. B. R. Boruah, and M. A. A. Neil, "Far field computation of an arbitrarily polarized beam using fast Fourier transforms," *Opt. Commun.* **282**(24), 4660–4667 (2009).
12. M. Born, and E. Wolf, *Principles of Optics*, (Cambridge University Press, Cambridge, UK, 1999).
13. R. Kant, "An analytical solution of vector diffraction for focusing optical systems with Seidel aberrations I. Spherical aberration, curvature of field, and distortion," *J. Mod. Opt.* **40**(11), 2293–2310 (1993).
14. R. Kant, "An analytical method of vector diffraction for focusing optical systems with Seidel aberrations II: Astigmatism and coma," *J. Mod. Opt.* **42**(2), 299–320 (1995).
15. R. K. Singh, P. Senthilkumaran, and K. Singh, "Effect of primary spherical aberration on high-numericalaperture focusing of a Laguerre-Gaussian beam," *J. Opt. Soc. Am. A* **25**(6), 1307–1318 (2008).
16. R. K. Singh, P. Senthilkumaran, and K. Singh, "Focusing of a vortex carrying beam with Gaussian background by an apertured system in presence of coma," *Opt. Commun.* **281**(5), 923–934 (2008).
17. R. K. Singh, P. Senthilkumaran, and K. Singh, "Focusing of linearly-, and circularly polarized Gaussian background vortex beams by a high numerical aperture system afflicted with third-order astigmatism," *Opt. Commun.* **281**(24), 5939–5948 (2008).
18. S. H. Deng, L. Liu, Y. Cheng, R. X. Li, and Z. Z. Xu, "Investigation of the influence of the aberration induced by a plane interface on STED microscopy," *Opt. Express* **17**(3), 1714–1725 (2009).

19. Y. Roichman, A. Waldron, E. Gardel, and D. G. Grier, "Optical traps with geometric aberrations," *Appl. Opt.* **45**(15), 3425–3429 (2006).
 20. B. Richards, and E. Wolf, "Electromagnetic diffraction in optical systems II: Structure of the image field in an aplanatic system," *Proc. R. Soc. Lond. A Math. Phys. Sci.* **253**(1274), 358–379 (1959).
 21. V. Westphal, and S. W. Hell, "Nanoscale resolution in the focal plane of an optical microscope," *Phys. Rev. Lett.* **94**(14), 143903 (2005).
 22. P. Dedecker, B. Muls, J. Hofkens, J. Enderlein, and J. Hotta, "Orientational effects in the excitation and de-excitation of single molecules interacting with donut-mode laser beams," *Opt. Express* **15**(6), 3372–3383 (2007).
 23. N. Bokor, Y. Iketaki, T. Watanabe, K. Daigoku, N. Davidson, and M. Fujii, "On polarization effects in fluorescence depletion microscopy," *Opt. Commun.* **272**(1), 263–268 (2007).
-

1. Introduction

In stimulated emission of depletion (STED) microscopy, two beams are combined to realize the super-resolution. One pump beam is used to excite the sample and another depletion pattern of a central zero-intensity distribution serving as a STED beam is used to suppress the fluorescence process at the periphery around the center through stimulated emission [1–3]. The degree of resolution enhancement of the STED microscopy is mainly dominated by the quality of the fluorescence depletion patterns. Generally, an ideal depletion pattern is hoped to be a null intensity surrounded with a high and steep intensity profile at the periphery. Several methods have been proposed to generate the required intensity distribution with one or several isolated regions of zero intensity [4–6]. Mostly in experiments, the effective inhibition patterns are generated by inserting appropriate phase mask in a Gaussian beam before transferring the beam into an objective lens. Three typical phase masks are often used in practice. To realize two-dimensional super-resolution on the focal plane in STED microscopy, a doughnut-shape distribution can be generated by transmitting the left-hand circularly (LC) polarized light through a vortex phase mask [7,8]. And a semi-circular or a central half-wavelength phase plate is used to produce a narrow line-shaped valley oriented in one lateral axis or in the optical axis [4].

Under realistic experimental conditions, it's inevitable to suffer wavefront aberrations even for the well-corrected objectives [9–11]. For instance, in the experimental arrangement, wavefront distortion produces from the reflection of light beams from an irregular surface of the dichromatic mirrors or passing through a filter of excessive wedge angles between its outer surfaces. Especially, the spherical aberration, coma and astigmatism are the primary aberrations encountered in experiments [12]. Spherical aberration frequently happens in optical microscope system and among the factors that can add spherical aberration there are poor quality immersion oil between the objective and specimen, the specimen mounting medium or the specimen itself. Also, coma is primarily an off-axis aberration and it has adverse impacts to microscope systems which commonly utilize laser scanning. Astigmatism can be increased by the misalignments in the optical path of the microscope.

As a result, the study of the influences of the aberrations on the lens system has drawn much attention. The deduction of aberration functions has been previously investigated in the literature [12–14]. Based on their research, the influence of primary aberrations on the polarization of focused radially polarized beams has been investigated in paper of [9]. And the group of R. K. Singh gave a detailed analysis for the effects of moderate amounts of spherical aberration, coma and astigmatism on the focusing field of a high numerical aperture (NA) system of Laguerre-Gaussian (LG) beams with different topological charge m [15–17]. Also, the sensitivity of singular light beams to azimuthal aberrations has been shown in paper of [10]. Using fast Fourier transform (FFT) operations, the focal field components of an arbitrarily polarized beam were detailedly computed in the presence of a number of Zernike mode aberrations [11]. The effects of aberration on the STED microscopy were also studied by some researchers. The change of STED generation volume of using the de-excitation pattern created by a phase plate of central $\lambda/2$ phase retardation aberrated by a glass to water interface was previously analyzed [8]. And in another paper of [18], the effects of aberration produced by focusing beams through an interface between the media of the mismatched refractive indices on the shape of depletion patterns and the size of fluorescence emission spot

in the STED microscopy were detailedly discussed. Moreover, the influences of geometrical aberrations on the in-plane performance of optical traps were also studied [19].

In view of the importance of the depletion patterns in STED microscopy and since the presence of aberration will lead to the structural modification of focused spot [9], we have explored the effects of the primary aberrations including the spherical aberration, the coma and the astigmatism on the three depletion patterns mentioned above in this paper.

2. Theory

By transmitting a Gaussian beam through an appropriate phase mask and focusing the beam with a high-NA objective lens, a depletion pattern of dark center can be obtained. The amplitude of the Gaussian beam at the input plane can be represented by the function of the conic angle θ and the polar coordinate ϕ as follows

$$E_0(\gamma, \theta) = A_0 \exp(-\gamma^2 \frac{\sin^2 \theta}{\sin^2 \alpha}) \quad (1)$$

where A_0 is the amplitude, $\gamma = a_0 / \omega_0$ is the truncation parameter with a_0 as the aperture radius and ω_0 denoting the beam size at waist. α represents the maximal semi-aperture angle of the objective. According to the vectorial Debye theory [20], when a linearly-polarized monochromatic beam is focused by a high NA objective lens, the diffracted field of the point p near focus is given as

$$E(p) = \begin{pmatrix} E_x \\ E_y \\ E_z \end{pmatrix} = -\frac{if}{\lambda} \int_0^\alpha \int_0^{2\pi} E_0 \sqrt{\cos \theta} A_1(\theta, \phi) \exp[ik(x \sin \theta \cos \phi + y \sin \theta \sin \phi + z \cos \theta)] \times \varphi_s(\theta, \phi) \begin{bmatrix} \cos \theta \cos^2 \phi + \sin^2 \phi \\ \cos \phi \sin \phi (\cos \theta - 1) \\ -\sin \theta \cos \theta \end{bmatrix} \sin \theta d\theta d\phi \quad (2)$$

Here f is the focal length of the lens, λ and $k = 2\pi n / \lambda$ are the wavelength in vacuo and the wave number, respectively. n is the refractive index. (x, y, z) are the Cartesian coordinates of the point p in the focal region. $A_1(\theta, \phi)$ denotes the wavefront aberration function and usually three primary aberrations in the beam can be expressed as [12–14]

$$\text{spherical aberration: } A_1(\theta, \phi) = \exp[ikA_s (\frac{\sin \theta}{\sin \alpha})^4] \quad (3)$$

$$\text{coma: } A_1(\theta, \phi) = \exp[ikA_c (\frac{\sin \theta}{\sin \alpha})^3 \cos \phi] \quad (4)$$

$$\text{astigmatism: } A_1(\theta, \phi) = \exp[ikA_a (\frac{\sin \theta}{\sin \alpha})^2 \cos^2 \phi] \quad (5)$$

where all the aberration coefficients A_s , A_c and A_a are in units of the wavelength of the beam. $\varphi_s(\theta, \phi)$ is the phase delay of the phase mask imposed on STED beam in the system.

By use of electric field distribution of the x - and y -polarized gauss beam, we obtain the filed distribution of the circularly polarized light in the focal plane [15]. For left-handed circularly polarized Gaussian beam, the components of the electric field at focus are expressed as

$$E(p) = \begin{pmatrix} E_x \\ E_y \\ E_z \end{pmatrix} = -\frac{if}{\lambda} \int_0^\alpha \int_0^{2\pi} E_0 \sqrt{\cos \theta} A_1(\theta, \phi) \exp[ik(x \sin \theta \cos \phi + y \sin \theta \sin \phi + z \cos \theta)] \times \varphi_s(\theta, \phi) \begin{bmatrix} \cos \theta \cos^2 \phi + \sin^2 \phi + i \sin \phi \cos \phi (\cos \theta - 1) \\ \cos \phi \sin \phi (\cos \theta - 1) + i (\cos \theta \sin^2 \phi + \cos^2 \phi) \\ -\sin \theta (\cos \theta + i \sin \phi) \end{bmatrix} \sin \theta d\theta d\phi \quad (6)$$

The intensity point spread function (I-PSF) is therefore given as $I(p) = |E_x|^2 + |E_y|^2 + |E_z|^2$.

When an erase beam is used in STED microscopy, the fluorescence of sample are exponentially depleted with the intensity of depletion light and the diameter d of the obtained sub-diffraction spot is approximately follows [3, 21]

$$d \approx \lambda / \left(2NA \sqrt{1 + I_{STED}^{\max} / I_s} \right) \quad (7)$$

In (7), I_{STED}^{\max} is the maximum intensity of the inhibition light and I_s represents the characteristic saturation intensity.

3. Results and discussion

In the following examples, the results are presented using an oil immersion objective lens with $NA = 1.4$ ($\alpha = 67.3^\circ$). Assumption of $\gamma = 1$ in our numerical simulations means that the aperture of the objective lens is fulfilled by a Gaussian beam and this requirement is usually met in practical experiments to obtain the best resolution and make full use of the laser power. The complex amplitudes of the linearly and circularly polarized beam at the focus can be calculated according to the Eq. (2) and Eq. (6). All the results are normalized by the maximum intensity of the aberration free case. In practical applications, the vortex phase (VP) plate is usually inserted in a LC polarized Gaussian beam for the perfect zero intensity with an annular intensity profile, shown in Fig. 1(a). And a helical phase delay $\varphi_s(\theta, \phi) = \exp(i\phi)$ ($0 \leq \phi \leq 2\pi$) is induced when using such a vortex mask [7].

Another phase plate induces a phase lag of π between the two equal parts of the incoming wave front corresponding to the phase retardation $\varphi_s(\theta, \phi) = \exp[i \times \text{sign}(\sin \phi) \pi / 2]$ [4]. And an x -polarized gauss beam is often transmitted through such a semi-circular $\lambda / 2$ phase (SCP) mask to form a narrow zero-valley oriented in a lateral axis, as shown in Fig. 2(a).

The pattern of the third phase mask consisting of a central circular area with a π -phase retardation is identified as the best de-excitation light for confinement of the fluorescence spot in the axial direction and its phase function is $\varphi_s(\theta, \phi) = \exp\{i \times \text{sign}[\sin(\theta - \theta_0)] \pi / 2\}$ with $\theta_0 = \arcsin(0.618 \sin \alpha)$ [22]. Figure 3(a) displays its intensity distribution featuring two maxima on the optical axis when using such a central half-wavelength phase (CP) plate in LC polarized Gaussian beam.

Using these three depletion patterns, the STED microscope can increase the resolution in the xy plane, along one lateral direction and on the axis direction, respectively. It is noted that the efficiency of fluorescence depletion in STED microscopy depends on the relative polarizations of pump and erase beams. Consequently, the pattern generated by inserting a SCP plate in linearly polarized beam works most effectively when the pump, erase fields and the molecular transition dipole are all parallel [22,23]. Since vortex phase plate allows for best alignment of the two beams in STED microscope and highest lateral resolution, the effects of aberrations on its pattern draw more attention.

3.1 Intensity distribution aberrated with spherical aberration

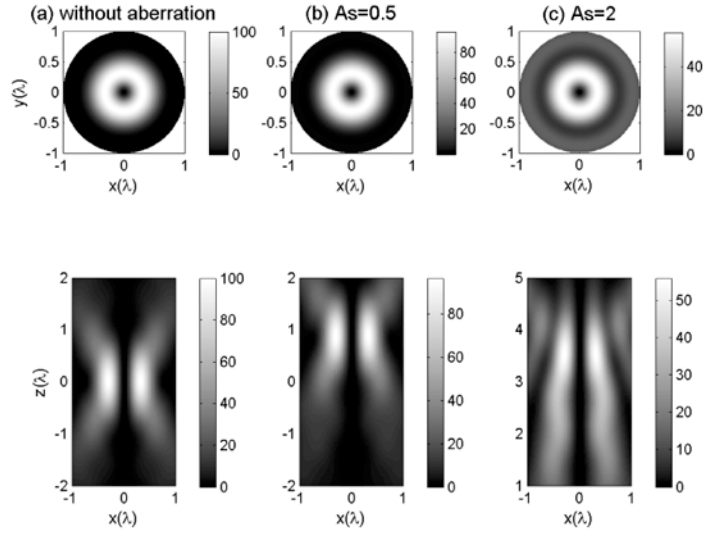


Fig. 1. Calculated intensity distribution on the focal plane and through the focus of a LC polarized Gaussian beam inserted with the vortex mask for different spherical aberration: (a) without aberration, (b) $A_s = 0.5$, (c) $A_s = 2$.

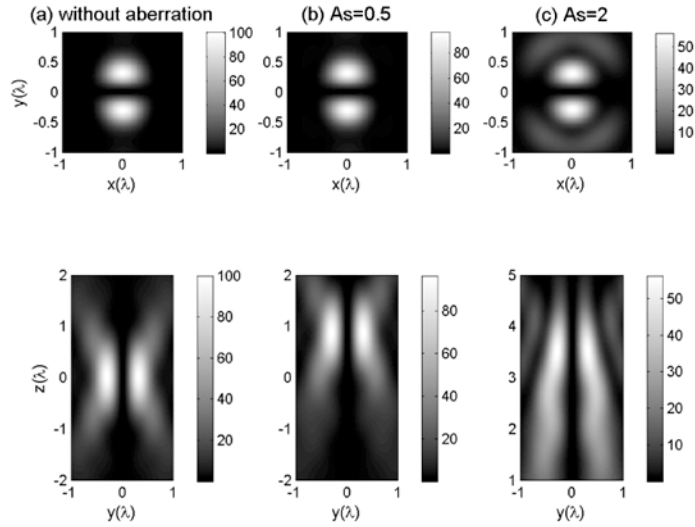


Fig. 2. Calculated intensity distribution on the focal plane and through the focus of a linearly polarized Gaussian beam inserted with the semi-circular $\lambda/2$ phase mask for different spherical aberration: (a) without aberration, (b) $A_s = 0.5$, (c) $A_s = 2$.

In the case of the pattern created by a VP plate inserted in a LC polarized Gaussian beam being suffered with the spherical aberration, the diffraction field in the focus can be expressed as integral of Bessel function $J_m(k\rho \sin \theta)$ with $\rho = \sqrt{x^2 + y^2}$ since the spherical aberration is only the function of θ [18,20]. And we can conclude from that the symmetry of the central dark hole on the focal plane is always maintained for moderate amount of spherical aberration. This conclusion is clearly manifested in Fig. 1, which shows the intensity distributions in the focal plane (xy plane) and through focus (xz plane) for the aberration-free

case and with different spherical aberration: $A_s = 0.5$, $A_s = 2$. From this figure, it can be seen that the shape of this pattern remains reasonably stable. And more importantly, the size of the dark hole and zero-intensity of center are almost unchanged. It's also noted that the presence of this aberration reduces the maximum intensity at the periphery resulting in reduction in the sharpness of the dark core. According to the Eq. (7), the corresponding resolution of STED system decreases. At the same time, the position of the intensity peak in the sidelobes shifts from the geometrical focal point and intensity lobes stretches along z axis [Fig. 1(b-c)]. Moreover, the focal shift and the stretching increase with an increment in A_s .

Intensity distributions in case of an x -polarized gauss beam inserted with a SCP mask are shown in Fig. 2. As a result, a narrow line-shaped valley oriented in the x axis is formed and this model is expected to predict efficient fluorescence depletion along y axis, which can be seen from Fig. 2(a). Similar influences of the spherical aberration on this pattern are obtained, shown in Fig. 2(b-c). The shape and the zero-center are still maintained. It also leads to the decrease of the maximum intensity and the focal shift along the optical axis. As this figure shows, the effect of such aberration is small for this pattern.

Using the CP plate in LC circularly polarized Gaussian beam produces an inhibition pattern to obtain a narrower fluorescence spot in z direction [Fig. 3(a)]. The most pronounced effect of spherical aberration on this pattern is the intensity maximums of the two separated spots become asymmetric along with a positional displacement of the dark core on the optical axis, shown in Fig. 3(b-c). Also the distance of the brighter portions of this pattern increases with increasing the spherical aberration, which is obviously manifested by the line profiles through central zero intensity of this pattern, as shown in Fig. 3(d). In this figure, for better contrast, all the profiles are dealt with to keep the zero-intensity point at the origin. The zero intensity of the dark hole is also found to be maintained for moderate amount of the spherical aberration. Consequently, an asymmetric and extended fluorescence spot of STED microscopy along z axis can be obtained when this pattern is applied with the spherical aberration.

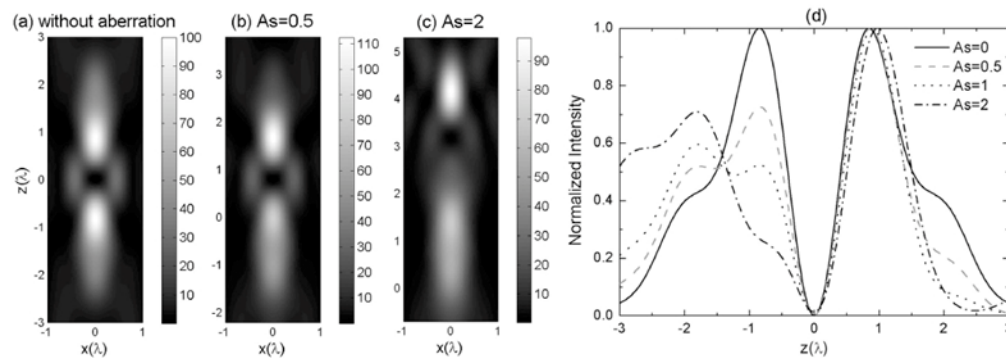


Fig. 3. Calculated intensity distribution on the xz plane of a LC polarized Gaussian beam inserted with the central $\lambda/2$ phase mask for different spherical aberration: (a) without aberration, (b) $A_s = 0.5$, (c) $A_s = 2$. Figure (d) is normalized intensity profiles through central zero intensity of this pattern for different spherical aberrations.

3.2 Intensity distribution aberrated with coma

The influences of coma on the intensity distribution of the three patterns mentioned above are depicted in Fig. 4, Fig. 5 and Fig. 6, respectively. From these figures, it is clearly noticed that the presence of coma produces the positional displacement of the dark center of all the three patterns on the x axis along with the decrease of peak intensity and the stretching on the optical axis with increase of the coma coefficient. Especially, the effects of the coma on the depletion patterns created by vortex mask [Fig. 4] and CP plate [Fig. 5] in a LC circularly

polarized gauss beam are serious. Compared with the aberration-free case, the rotational symmetry of the hole vanishes and the annular intensity profile is compressed in one side on the focal plane for the pattern of vortex mask in the presence of coma, shown in Fig. 4, which in turn an asymmetric and extended fluorescence spot produces when applying this pattern in STED microscope.

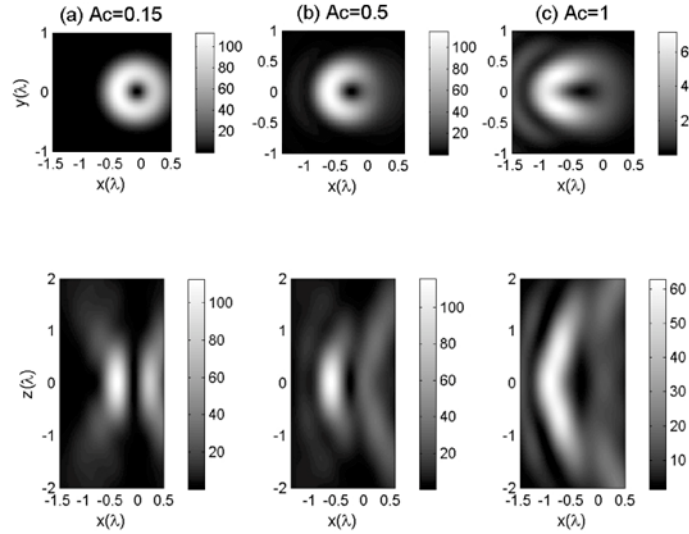


Fig. 4. Calculated intensity distribution on the focal plane and through the focus of a LC polarized Gaussian beam inserted with the vortex mask for different coma: (a) $A_c = 0.15$, (b) $A_c = 0.5$, (c) $A_c = 1$.

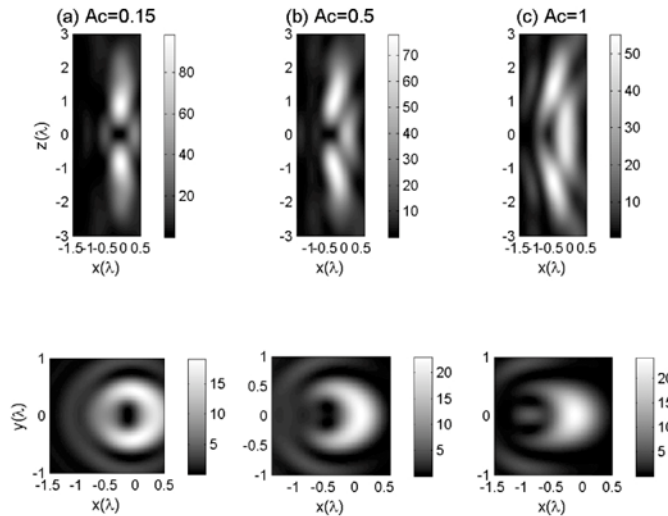


Fig. 5. Calculated intensity distribution through the focus and on the focal plane of a LC polarized Gaussian beam inserted with the central $\lambda/2$ phase mask for different coma: (a) $A_c = 0.15$, (b) $A_c = 0.5$, (c) $A_c = 1$.

For the inhibition pattern created by a CP plate, higher coma modifies the structure into a conic shape [Fig. 5(c)]. Moreover, the minimum intensity of the dark hole no longer remains zero and the residual intensity at the center of the hole elevates with increasing value of A_c ,

which correspondingly weakens the fluorescence in the center and limits further enhancement of the resolution achieved in STED microscopy. In this plot, the residual intensity at the dark center is about 4.81% of the maximum intensity with $A_c = 0.5$ and increases to 22.7% with $A_c = 1$.

It must be noted in Fig. 6 that the shape of a dark valley with the distribution of two maxima on y direction is reasonably preserved in the case of SCP plate and the data shows that the zero intensity of the center is always maintained regardless of moderate amount of coma aberration introduced in the system. Also the broadening effect of two brighter portion caused by the coma is obvious only for higher value of A_c , as displayed in Fig. 6(d), which is the picture of line profiles through central zero intensity of this pattern. As a result, the effect of coma is less pronounced on this pattern.

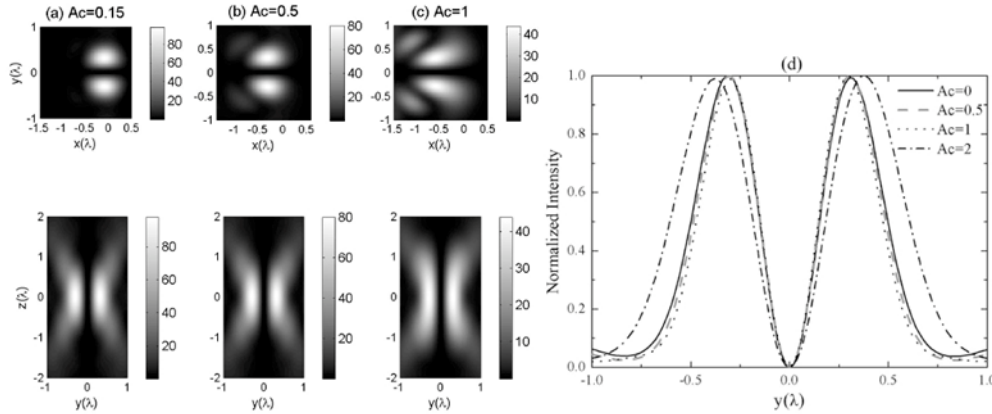


Fig. 6. Calculated intensity distribution on the focal plane and through the focus of a linearly polarized Gaussian beam inserted with the semi-circular $\lambda/2$ phase mask for different coma: (a) $A_c = 0.15$, (b) $A_c = 0.5$, (c) $A_c = 1$. Figure (d) is normalized intensity profiles through central zero intensity of this pattern for different coma.

3.3 Intensity distribution aberrated with astigmatism

The structures of the three patterns with astigmatism are shown in Fig. 7, Fig. 8 and Fig. 9 for $A_a = 0.15$, $A_a = 0.5$ and $A_a = 1$. From these figures, we also find that small positional displacement of the dark center of the three patterns on the optical axis occurs and the peak intensity decreases with an increment of the astigmatism coefficient. Figure 7 shows that the symmetric intensity ring of LC polarized beam with VP plate vanishes and is found to be split into two high-intensity lobes when higher astigmatism occurs [Fig. 7(b)]. Even for the smaller astigmatism of $A_a = 0.15$, the dark-hole intensity distribution is changed into a distribution of zero-intensity with two sidelobes [Fig. 7(a)]. And with an increment in the value of A_a , the brighter parts are elongated in a certain lateral direction [Fig. 7(c)]. It is obviously concluded that when the astigmatism is present in system, a doughnut-shape distribution disappears and this pattern can't work as normal to realize two-dimensional super-resolution in the focal plane in STED microscopy.

The astigmatism of the system also leads to a serious distortion of the structure of the pattern created by inserting a CP plate within a circularly polarized gauss beam, seen in Fig. 8. The distribution possesses a central non-zero intensity of the hole and the residual intensity continuously arises with increase of A_a . For a higher value of astigmatism, the effects are even more pronounced and this pattern is no longer considered as an effective depletion pattern to realize super-resolution along z axis in STED microscopy (Fig. 8(c)). Compared

with the effects of coma, the distortion of the structures of the pattern created by vortex mask or the CP plate is more serious in the presence of astigmatism.

The dark line-shaped valley and the zero-intensity still preserve in the inhibition pattern generated by using a SCP mask in linearly polarized gauss beam under the influence of astigmatism, shown in the intensity distribution on the focal plane and yz plane of Fig. 9. Also an increment of peak-to-peak separation is obviously seen with increasing the value of A_a in Fig. 9(d), in which the intensity profiles through the central zero of this pattern are depicted. Correspondingly, the size of the fluorescent spot in STED microscopy increases in the presence of astigmatism. In contrast with the effects of coma, we can find from Fig. 9 that the effects of astigmatism are more pronounced on this pattern.

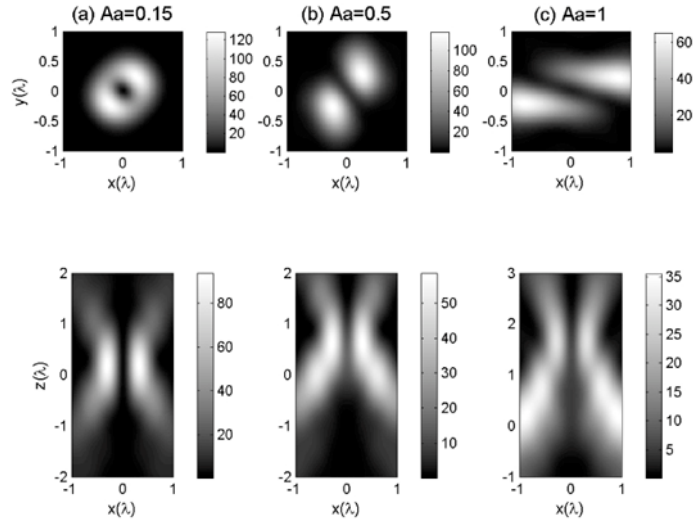


Fig. 7. Calculated intensity distribution on the focal plane and through the focus of a LC polarized Gaussian beam inserted with the vortex mask for different astigmatism: (a) $A_a = 0.15$, (b) $A_a = 0.5$, (c) $A_a = 1$.

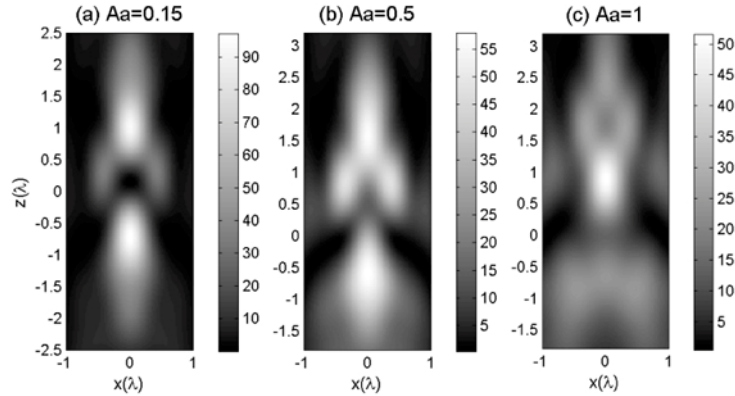


Fig. 8. Calculated intensity distribution on the xz plane of a LC polarized Gaussian beam inserted with the central $\lambda/2$ phase mask for different astigmatism: (a) $A_a = 0.15$, (b) $A_a = 0.5$, (c) $A_a = 1$.

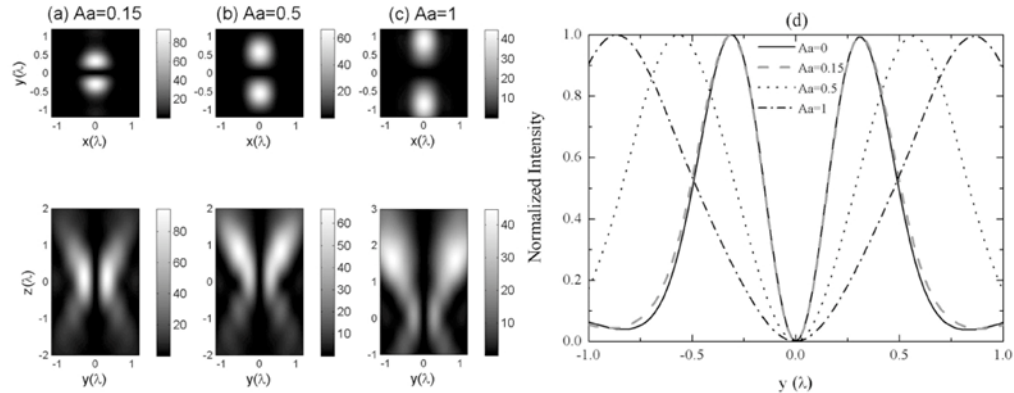


Fig. 9. Calculated intensity distribution on the focal plane and through the focus of a linearly polarized Gaussian beam inserted with the semi-circular $\lambda/2$ phase mask for different astigmatism: (a) $A_a = 0.15$, (b) $A_a = 0.5$, (c) $A_a = 1$. Figure (d) is normalized intensity profiles through central zero intensity of this pattern for different astigmatism.

4. Conclusion

In this paper, we analyze the effects of spherical aberration, coma and astigmatism on the three inhibition patterns mainly used in STED microscopy. These depletion patterns are created by inserting a vortex phase (VP) plate, central half-wavelength phase (CP) plate or a semi-circular half-wavelength phase (SCP) mask within a Gaussian beam respectively. The results obtained in our study are helpful to provide guidelines to make a judgment on what kind of aberration is playing the major role from the intensity distribution observed in practical experiments.

All the aberrations degrade the performance of STED system. We find that the spherical aberration has the least effects on the field of the three patterns mentioned above. Astigmatism and coma strongly distort the focal fields and particularly degrades the shape of the patterns generated by VP plate and CP plate. Especially, in the presence of astigmatism, the focal fields are already so distorted that these two patterns probably would be useless for super-resolution optical microscopy. In contrast with the effects of coma, the effects of astigmatism are more pronounced on the three patterns. For STED system that highly depends on the structure of the inhibition patterns, coma and especially astigmatism are of great concern.

The three main depletion patterns are used for different purposes in STED microscope and display different sensitivities to the aberrations. For the depletion pattern of SCP mask, the basic shape and the zero intensity are always maintained under the influence of moderate amount of primary aberrations, which means that this pattern has lower aberration sensitivity. The pattern of a doughnut shape created by a VP plate has a larger sensitivity to the coma and astigmatism and as a result, this pattern apparently requires more attention when applied in experiments. The inhibition pattern of a CP plate is also sensitive to a certain amount of spherical aberration and coma, but smaller amount of astigmatism will substantially degrade its intensity distribution at focus.

Acknowledgments

This work is financially supported by the National Natural Science Fund (NO. 60527004) of China.